High-Resolution Structure of the Diphtheria Toxin Repressor Complexed with Cobalt and Manganese Reveals an SH3-like Third Domain and Suggests a Possible Role of Phosphate as Co-corepressor[†,‡]

Xiayang Qiu,[§,||] Ehmke Pohl,[§] Randall K. Holmes,[⊥] and Wim G. J. Hol*[,§,#]

Department of Biological Structure, Biomolecular Structure Program, and Howard Hughes Medical Institute, P.O. Box 357370, School of Medicine, University of Washington, Seattle, Washington 98195, and Department of Microbiology, University of Colorado Health Sciences Center, Denver, Colorado 80262

Received April 10, 1996; Revised Manuscript Received June 25, 1996[⊗]

ABSTRACT: The crystal structure of diphtheria toxin repressor (DtxR) in complex with the corepressor Co^{2+} has been determined at 2.0 Å resolution and in complex with Mn^{2+} at 2.2 Å resolution. The structure of the flexible third domain could be determined at this high resolution. It appears to contain five antiparallel strands exhibiting a fold very similar to the SH3 domain. A superposition of 46 equivalent Cα atoms of DtxR and α-spectrin SH3 resulted in an rms deviation of 3.0 Å. The sequence identity is only 7%. This third domain of DtxR appears to have no interactions with the DNA binding domain nor with the metal binding domain of the repressor. Yet, flexibility in the region between the second and the third domain allows in principle significant conformational changes such as might occur upon DNA binding. The two metal binding sites in the second domain have been unraveled in considerable detail. Metal binding site 1 was well occupied in both the cobalt and manganese structures and showed a surprising sulfate ion as ligand. The sulfate was proven beyond doubt by the high peak at its position in a selenate versus sulfate difference Fourier. The presence of the intriguing sulfate ion at such a crucial position near the metal corepressor suggests the possibility that under physiological conditions phosphate may act as a "co-corepressor" for this class of metal-regulated DNA binding proteins in Corynebacteria, Mycobacteria, and related organisms. The second metal binding site is significantly different in these two DtxR structures. In the 2.0 Å cobalt structure, the site is not occupied by a metal ion. In the 2.2 Å manganese structure the site is well occupied, at approximately the same position as observed previously in cadmium DtxR. The ligands are Glu105, His106, the carbonyl oxygen of Cys102, and a water molecule. The reasons for differential occupancy of this site in different structures are intriguing and require further investigations.

Iron is an essential nutrient for almost all the bacteria, but the availability of free iron in mammalian hosts is extremely limited, serving as a defense mechanism against infection (Weinberg, 1993). Siderophore synthesis is the major component of the highly evolved iron-uptake machinery that is crucial to the survival of pathogenic bacteria in the host. Interestingly, low iron conditions in humans are used as signals for the synthesis of virulence factors by a wide variety of pathogenic bacteria. It is therefore not surprising that iron-activated repressors have been identified in most of the bacteria, globally regulating their iron-uptake and virulence factor productions (Litwin & Calderwood, 1993). In *Corynebacterium diphtheriae*, in the presence of about 1 μM ferrous ions in the culture medium, diphtheria toxin repressor (DtxR) becomes activated (Barksdale, 1970). The active dimeric repressor can interact very strongly and specifically with the *tox* and *irp* operators (Schmitt *et al.*, 1992; Schmitt & Holmes, 1994). Several important proteins, such as diphtheria toxin and the siderophore synthesis enzymes, are encoded by the *tox* and *irp* genes. The transcription initiation sites of these genes are blocked by the formation of the stable repressor−Fe^{2+}−DNA ternary complexes so that the production of virulence factors by *C. diphtheriae* is repressed at higher Fe^{2+} concentration (Boyd *et al.*, 1990; Schmitt *et al.*, 1992).

Functionally homologous repressor proteins have recently been characterized for *Brevibacterium lactofermentum* and *Mycobacterium tuberculosis*, emphasizing the importance of this type of protein (Oguiza *et al.*, 1995; Schmitt *et al.*, 1995).

To understand the function of the diphtheria toxin repressor, several major questions have to be addressed, such as the mode of dimer formation, metal coordination, and DNA recognition, as well as the mechanism of its iron-activated DNA binding. We reported recently the 2.8 Å crystal structures of DtxR in complex with six divalent transition metal cation corepressors (Qiu *et al.*, 1995). It was the first structure of an iron-activated DNA binding protein, as well as the first structure in the class of iron-dependent repressors. The 3.0 Å structure of Apo DtxR in a different space group has been independently solved and published by Schiering

[†] This work was supported by the National Institutes of Health to W.G.J.H. (R01CA65656) and R.K.H. (R01AI14107) and Fellowship Grant GM16713 to X.Q. W.G.J.H. is indebted to the Murdock Charitable Trust for a major equipment grant to the Biomolecular Structure Center. E.P. is grateful to the Schering Forschungsgesellschaft for a postdoctoral fellowship.

[‡] Atomic coordinates of the diphtheria toxin repressor have been deposited in the Brookhaven Protein Data Bank with access code 2DTR.

* To whom correspondence should be addressed.

[§] Department of Biological Structure, Biomolecular Structure Program, University of Washington.

[||] Current address: Department of Macromolecular Sciences, SmithKline Beecham Pharmaceuticals, Mail Code UE0447, 709 Swedeland Road, King of Prussia, PA 19406-0939.

[⊥] University of Colorado Health Sciences Center.

[#] Howard Hughes Medical Institute, University of Washington.

[⊗] Abstract published in *Advance ACS Abstracts,* August 1, 1996.

S0006-2960(96)00861-6 CCC: $12.00

et al. (1995). DtxR consists of three domains. The N-terminal domain of DtxR was found to contain a classical helix−turn−helix (HTH) motif, which is often responsible for DNA recognition in DNA binding proteins. The second domain was identified to be the dimerization domain, containing also the ligands for the two metal binding sites. The third domain of about 80 amino acids was largely invisible at 2.8 Å resolution in our DtxR−metal complexes (Qiu *et al.*, 1995) as well as in the apo structure (Schiering *et al.*, 1995).

Diphtheria toxin repressor recognizes about 30 base pairs of pseudopalindromic sequences within the *tox* or *irp* operators. A DtxR dimer has been proposed to bind DNA (Qiu *et al.*, 1995) in a manner similar to the CAP (catabolite gene activator protein)−DNA interaction (Shultz *et al.*, 1990). While Fe^{2+} is the physiologically relevant and most potent corepressor of the diphtheria toxin repressor, Mn^{2+}, Co^{2+}, Ni^{2+}, and Cd^{2+} are all able to function as corepressor and activate DtxR *in vitro* (Tao & Murphy, 1992; Schmitt *et al.*, 1992; Schmitt & Holmes, 1993). The repressor can also be activated weakly by Zn^{2+}; however, this requires at least a 100 μM metal ion concentration, i.e., approximately 2 orders of magnitude more than the amount of Fe^{2+} needed to obtain active holorepressor (Wang *et al.*, 1994).

The DtxR structures of Qiu *et al.* (1995) revealed two metal binding sites for divalent transitions metal ions which can function as corepressor. One of these, metal binding site 1, was well occupied in all six structures studied. The second site was only occupied in the Cd^{2+}−DtxR structure and in the mercury derivatives (Qiu *et al.*, 1995). A mercury derivative of Schiering *et al.* (1995) showed that mercury also occupies metal binding site 1, while several mercury binding sites were distributed near binding site 2. The limited resolution of the mercury derivatives did not permit a detailed description of the mercury sites, however.

The current paper describes well-refined structures of the diphtheria toxin repressor complexed with Co^{2+} and Mn^{2+} at 2.0 and 2.2 Å, respectively. This allowed a virtually complete description of the third DtxR domain. In addition, these structures provide new information about the coordination of metal binding site 1 and show that Mn^{2+} occupies metal binding site 2 at significant levels. The consequences of these observations for our understanding of metal binding by the repressor are discussed.

MATERIALS AND METHODS

Protein Preparation, Purification, and Crystallization. Diphtheria toxin repressor was prepared and purified as described previously (Schmitt *et al.*, 1992; Schmitt & Holmes, 1993). Crystals of DtxR in complex with various divalent metal corepressors were obtained using hanging drops equilibrating against a well solution of 0.1 M Tris buffer and 1.8 M ammonium sulfate at pH 8.5 as reported (Qiu *et al.*, 1995).

Crystallographic Data Collection. Diffraction data from a large Co^{2+}−DtxR crystal (0.7 mm × 0.4 mm × 0.4 mm) were collected at room temperature using an Raxis-II imaging plate system on a Rigaku RU-200 rotating anode X-ray source. The crystal diffracted to approximately 2.0 Å resolution. The crystal belongs to the trigonal space group $P3_121$, with unit cell dimensions of $a = b = 63.9$ Å and $c = 109.3$ Å. There is one monomer per asymmetric unit, and the calculated solvent content is 52% with $V_m = 2.6$ Å^3/D. A total of 14 788 independent reflections were obtained from 41 868 observations, with R_{merge} being 0.045. The data set is 78% complete to 2.0 Å (Table 1), with the last resolution shell (from 2.25 to 2.00 Å) being 52% complete and the average $I/\sigma(I)$ greater than 2. Some useful reflections between 2.0 and 1.9 Å were also collected and used later in the structure refinement and electron density map calculations.

Table 1: Statistics for Crystallographic Structure Determinations

data collection		
crystal	Co^{2+}−DtxR	SeO_4^{2-}−Mn^{2+}−DtxR
unit cell (Å)	$a = b = 63.9$, $c = 109.3$	$a = b = 64.0$, $c = 108.9$
resolution (Å)	50.0−1.9	50.0−2.2
observations	41868	36125
unique reflections	14788	11201
completeness (%)	78	81
R_{merge} (%)[a]	4.5	9.0
refinement		
resolution (Å)	7.0−1.9	7.0−2.2
unique reflections	14336	10736
R-factor (%)[b]	17.1	16.4
protein atoms	1666	1666
water molecules	150	120
anions	1	1
cations	1	2
rms bond length (Å)	0.012	0.012
rms bond angle (deg)	1.7	1.7
rms dihedral angle (deg)	22.5	22.3
rms improper angle (deg)	1.4	1.4

[a] $R_{merge} = \Sigma|I - \langle I\rangle|/\Sigma\langle I\rangle$. [b] R-factor $= \Sigma|F_o - F_c|/\Sigma F_o$.

Mn^{2+}−DtxR crystals were grown under virtually identical conditions as the cobalt-containing crystals and were subsequently transferred to a solution containing 0.5 mM $MnCl_2$ and 2.0 M Na_2SeO_4. A complete data set was collected using the same instruments and protocols just described. The crystal diffracted to 2.2 Å resolution. The crystal is isomorphous to the Co^{2+}−DtxR crystal, with unit cell dimensions being $a = b = 64.0$ Å and $c = 108.9$ Å. A total of 11 201 unique reflections were obtained from the 36 125 collected observations, with R_{merge} being 0.09. The overall data set is 81% complete to 2.2 Å (Table 1), with the last resolution shell (from 2.25 to 2.20 Å) being 61% complete and the average $I/\sigma(I)$ greater than 2. Both data sets were processed with the Raxis software.

Structure Determination and Refinement. Even though we could start from the 2.8 Å resolution structure of Fe^{2+}−DtxR, the refinement of the Co^{2+}−DtxR structure was achieved only with considerable effort consisting of very gradual improvements through a large number of iteration cycles. With all the data in the 10.0−2.8 Å range, the *R*-factor did quickly drop to about 0.25 through cycles of positional refinement and tightly restrained individual temperature factor refinement using the program X-PLOR (Brünger *et al.*, 1987). However, further improvements of the model depended largely upon the structure determination of the third domain, which has significantly higher temperature factors than the first two domains but is not completely disordered. In the 2.8 Å structure only 24 residues were located in the electron density maps. It is only after the inclusion of the high-resolution data that we were able to identify the rest of the third domain gradually from the difference electron density maps. At 2.8 Å only a few water molecules could be identified, and individual temperature factors were not

refined accurately. Using higher resolution data many solvent molecules could be included in the refinement, and the refinement of individual temperature factors became more reliable. Using difference Fourier maps as well as the sigma-weighted electron density maps (Read, 1986), calculated with combined phases from MIR and the partial model, two extra β-strands were built in as polyalanines. Inclusion of these two strands in the refinement further improved the phases and hence the resulting electron density maps. This progress is illustrated in Figure 3, which shows simulated annealing omit maps from a loop region around residue 208. Using X-PLOR, the subsequent refinement involved alternating cycles of positional refinement, restrained individual temperature factor refinement, and simulated annealing using slow cooling protocols. It also involved the calculation and analysis of numerous electron density maps, difference maps, and omit maps, gradually extending the resolution of the data included, adding solvent molecules and extensive model building on computer graphics with the program O (Jones *et al.*, 1991). The program ARP (Lamzin & Wilson, 1993) was also used in certain stages of the refinement and assisted in localizing extra protein residues and solvent molecules. Weak or missing electron density in simulated annealing omit maps (Hodel *et al.*, 1992) was observed for a number of residues in the highly mobile loop regions of this domain; there are breaks in the main chain at Ile153, Ser158, Gly191, Ala198, Asn207, and Gly208, while the side chains of Ala155, Lys162, Lys209, and Asp210 have only weak electron density. Arg60, Lys121, Ser158, and Met159 have been refined as alanines. The final structure is refined using all the 14336 reflections between 7.0 and 1.9 Å resolution, and the final *R*-factor is 0.171 with very acceptable geometry, 150 water molecules, one divalent cation, and a sulfate ion (Table 1).

The $Mn^{2+}-SeO_4^{2-}-$DtxR structure was determined using the refined 2.0 Å resolution $Co^{2+}-$DtxR structure as the initial model. Including all the 10 736 reflections in the 7.0−2.2 Å resolution range, the structure refinement required very little manual intervention and was virtually completed after only a few cycles of energy minimization and rebuilding of the water structure using X-PLOR. The final *R*-factor is 0.164 with very acceptable geometry, including two cations and one anion (Table 1). The second metal, refined with half-occupancy, obtained a temperature factor of 23 $Å^2$.

RESULTS

Quality of the Structure. The final model for both structures is 95% complete, missing only the N-terminal residues 1−3, the flexible linker 141−147 between domains 2 and 3, and residues 199−200 in a small loop connecting two of the β-strands in the third domain. The program PROCHECK (Laskowski *et al.*, 1993) was used to check for geometric outliers and showed that all 217 residues are in the allowed regions in the Ramachandran plot, with 93.7% of the residues in the most favored regions. All geometric criteria are equally well or better satisfied than those of the average acceptable structures determined at the same resolution.

The First Two Domains. Since the cobalt-containing structure has the highest resolution, data from that structure are mainly used for the following general protein description. Like the 2.8 Å $Fe^{2+}-$DtxR results, the 2.0 Å $Co^{2+}-$DtxR structure shows that each subunit can be divided into three

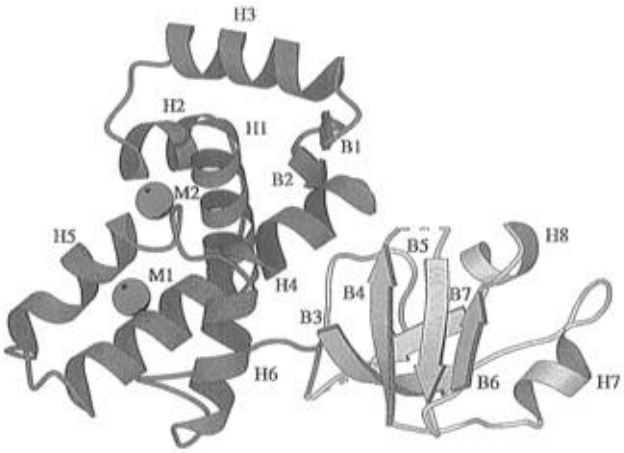

FIGURE 1: Structure of diphtheria toxin repressor in complex with Co^{2+} and Mn^{2+}. The N-terminal domain is shown in blue, the second domain in green, and the third domain in yellow. Secondary structure elements are labeled as α-helices H1 to H8 and β-strands B1 to B7, following the amino acid sequence from the N-terminus to the C-terminus. The two metal ions are shown in orange spheres, with the second metal from the Mn^{2+} structure. Dotted lines show the chain connections where residues are disordered and can not be seen in electron density maps. All figures have been prepared using the programs MOLSCRIPT (Kraulis, 1991) and O (Jones *et al.*, 1991).

domains (Figure 1). The first domain consists of amino acids Leu4−Thr73, with the three residues at the N-terminus being disordered even at 2.0 Å resolution. This domain is mostly α-helical except for a small β-hairpin loop between Val54 to Met64 comprising β-sheets B1 (Val54−Val56) and B2 (Leu62−Met64). There is an arginine, Arg60, at the tip of the β-hairpin, with its side chain pointing out to the solvent region and disordered in this structure. The N-terminal half (Pro66−Thr73) of the long helix H4 is also considered to be part of the first domain. The most important structural feature of this domain is the three-helix bundle (H1, Thr7−Glu20; H2, Arg27−Leu34; H3, Gly38−Arg50) that has been found to be similar to that of the DNA recognition domain of the catabolite gene activator protein (Qiu *et al.*, 1995; Shultz *et al.*, 1991). The term helix−turn−helix motif (HTH) has been used to classify this fold found in CAP and several other DNA binding proteins (Brennan, 1993). It usually contains a two to three turn helix (H2), a three to four residue turn (T), and a four-turn helix (H3), in which the two helices cross each other at an angle of approximately 120°. Although variations in the angle and lengths of the helices do occur in different proteins, helix H3 is always the DNA recognition helix that is embedded in the DNA major groove and is responsible for making many, but certainly not all, base-specific DNA contacts. The superposition of H2 and H3 of DtxR to the respective helices of CAP gave a deviation of only 0.7 Å in their Cα coordinates. In this structure of the diphtheria toxin repressor, it is worth noting that the turn in the HTH motif has only three residues, and the third helix H3 starts with a quite unusual Gly-Pro sequence. It is not clear whether these would lead to any kind of unusual stability of the structure motif, but if they would, it could play a role in the iron-activated DNA binding mechanism. Similar to other HTH motifs, helix H3 of diphtheria toxin repressor was proposed to be the DNA recognition helix (Qiu *et al.*, 1995), which agreed well with the results from biochemical and mutagenesis studies.

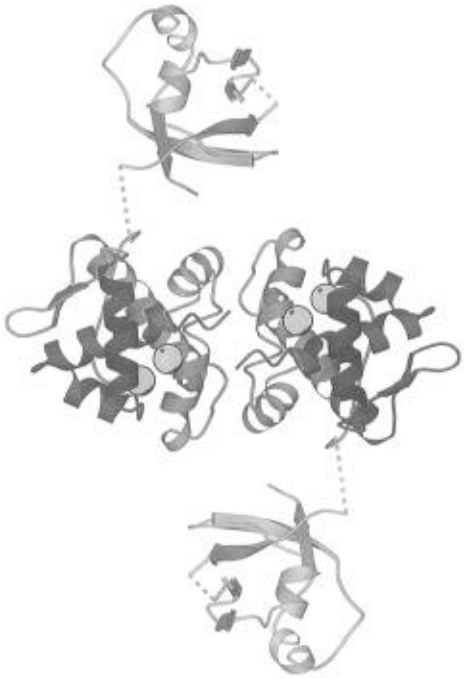

FIGURE 2: Structure of the DtxR dimer viewing along the crystallographic 2-fold axis. Dotted lines indicate the chain connections where residues are disordered and can not be seen in electron density maps

The second domain starts from Ala74 and ends at Val140 (Figure 1). Two metal binding sites were located in this domain of the Cd^{2+}−DtxR (Qiu *et al.*, 1995) and the Mn^{2+}−DtxR (see below) structures. This domain is also mostly helical, with the long helix H4 (Pro66−Asp88) connecting the core of the two domains. The second half of helix H4 provides two ligands (His79 and Glu83) for the first metal binding site M1. Helix H5 (Ile94−Trp104) is bent by about 30° and appears to be the center of several important functions of the repressor. It provides one ligand (His98) to the first metal binding site 1 and one ligand to the second metal binding site 2, whereas two other site 2 ligands (Glu105 and His106) are provided by two residues which immediately follow this helix. In fact, Glu105 and His106 seem to be part of the helix H5 by visual inspection, but the φ and ψ angles of Glu105 (−60.2°, −21.3°), and His106 (−90.4°, −13.7°) deviate too much from the ideal values to be accepted as helical residues. As will be discussed later, helix H5 is also the major component of the dimer interface, which is essential for the repressor activity (Figure 2). Helix H6 (Asp110−Val119) provides some additional residues to the dimer interface. The long loop afterward (Leu120−Val140) is also very well defined in the electron density maps, except for parts of the side chains of the last five residues. The loop contains a segment of a probably quite important nonapeptide with the sequence SPFGNPIPG, in which Ser126, Phe128, Asn130, and Pro131 all interact with the ligands or other residues in the vicinity of the first metal binding site.

The first two domains are well separated. There are very few direct interactions between the two, except for the long helix H4 linkage. All of the interdomain interactions involve residues from the first helix (H1). The side chain of Glu9 forms a salt bridge with the side chain of His106 (Glu9 OE1−His106 ND1, 3.2 Å), which is one of the ligands of metal binding site 2 in the Cd^{2+}− and Mn^{2+}−DtxR structures. The Arg13 side chain in its turn forms a pair of salt bridges with Glu105 (with the Arg13 NE−Glu105 OE1 and Arg13 NH2−Glu105 OE2 distances both being 3.0 Å), another ligand of metal binding site 2. Hence helix H1 has interactions with two ligands of metal binding site 2. Since helix H1 has also numerous interactions with the DNA recognition helix H3, these direct interactions between helix H1 and site 2 ligands are potentially of great functional importance. There is also a pair of salt bridges formed between Glu20 of the first domain and Arg80 of the second domain (Glu20 OE1−Arg80 NH2, 2.7 Å; Glu20 OE2−Arg80 NH1, 3.2 Å). Moreover, there is a close van der Waals interaction between Tyr16 of the first domain and Pro133, the distance being Tyr16 OH−Pro133 CB, 3.2 Å, which suggests that the Leu120−Val140 loop might be relevant to the stability of the repressor structure.

The SH3-like Third Domain. The third domain of diphtheria toxin repressor is highly flexible in the crystal. The average temperature factor of this domain is in both structures over 50 $Å^2$, compared to a value of about 30 $Å^2$ for the first two domains. At 2.8 Å resolution, only 24 residues could be located in the electron density maps for this 80-residue domain (Qiu *et al.*, 1995). The domain has now been identified for the first time after refinement at higher resolution, missing only a seven-residue linker between domains 2 and 3 and a two-residue loop connecting strands B4 and B5 (dotted lines in Figure 2). The seven-residue linker GNSDAAA consists of small amino acids, which is presumably the reason that the linker is too flexible to be seen even in the high-resolution electron density maps.

Unlike the first two domains that have a high α-helix content, the structure of the third domain (Figure 1) is mainly a pleated sheet of five antiparallel β-strands (B3, Arg161−Gln167; B4, Glu192−Asp197; B5, Ile202−His206; B6, Lys209−Glu212; B7, Ile221−Glu224). One side of the β-sheet is covered by two short helices (H7, Gln178−Leu183; H8, Asp215−Thr220) and connecting loops, while the other side is exposed to the solvent regions in the crystal. In the antiparallel β-sheet of this domain there are four hydrogen bonds found between each pair of adjacent strands, except for the case between strand B4 and strand B5 where one of the distances is 3.5 Å (Thr203 O−Val196 N), too far to be considered as a stable hydrogen bond. The hydrophobic core of this domain is composed of Val163, Ile165, and Ile168 of strand B4, Ala185 and Ile187 of a loop region, Val193 and Ile195 of strand B5, Ile202 and Leu204 of strand B6, Val211 of strand B7, Leu217 of helix H8, and Ile221 and Ile223 of strand B8. Several charged residues on the surface of the third domain have either disordered or poorly defined side chains, making quantitative analysis of the surface electrostatic potential less reliable. Overall, there are more negatively (16) than positively charged residues (11). However, positively charged surface regions do exist, with the most obvious cluster involving the side chains of Arg151, His219, and Arg222.

Using the computer program DALI (Holm & Sander, 1993), a search for known structures that are similar to the third domain has been performed against the Brookhaven Protein Data Bank. The third domain appears to exhibit a fold very similar to the SH3 domain of α-spectrin (Musacchio *et al.*, 1992). The rms deviation of 46 equivalent Cα atoms is 3.0 Å, and the sequence identity is only 7% (Table 2). The superposition of the third domain of DtxR and the

Table 2: Structure-Based Sequence Alignment of the Third DtxR Domain and the SH3 Domains of Spectrin, Fyn, and Abl[a]

		DtxR	spectrin	Fyn	Abl			DtxR	spectrin	Fyn	Abl
		M	·	·	·			·	T	S	H
160		**P**	**K**	V	P	200		**G**	**N**	E*	N
		R	**E**	T	N			H	K	G	G
	β	**K**	**L**	L	L			·	D	D*	E
	β	**V**	**V**	F	F		*β*	·	W	W*	W*
	β	**R**	**L**	V	V		*β*	**I**	**W**	W	C
	β	**I**	**A**	A	A		*β*	**T**	**K**	E	E
	β	**V**	**L**	L	L		*β*	**L**	**V**	A	A
	β	**Q**	**Y**	Y*	Y*		*β*	**S**	**E**	R	Q
		I	**D**	D	D		*β*	**H**	**V**	S	·
		N	Y	Y*	F*			**N**	**N**	L	·
170		E	·	·	·			·	·	T	T
		I	·	·	·			·	·	T	K
		F	·	·	·			**G**	**D**	G	N
		Q	·	·	·		*β*	**K**	**R**	G	G
		V	·	·	·	210	*β*	**D**	**Q**	T	Q
		E	·	·	·		*β*	**V**	**G**	G	G
		T	·	·	·		*β*	**E**	**F**	Y*	W
		D	E	E	V		*β*	**L**	**V**	I	V
	α	**Q**	**E**	A	A			L	·		
	α	**F**	**K**	R*	S*			D	·		
180	α	**T**	**S**	T*	G		α	D	·		
	α	**Q**	**P**	E	D*		α	L	·		
	α	L	R	D*	N		α	**A**	**P**	P*	P*
	α	L	E	D	T*		α	**H**	**A**	S	S
		D	V	L	L	220		**T**	**A**	N*	N*
		A	·	·	·		*β*	**I**	**Y**	Y*	Y*
		D	**T**	S	S		*β*	**R**	**V**	V*	I
		I	**M**	F	I		*β*	**I**	**K**	A	T
		R	**K**	H	T		*β*	**E**	**K**	P	P
		V	**K**	K	K		*β*	**L**	**L**	V	V
190		**G**	**G**	G	G			**L**	**D**	D	N
	β	S	D	E	E						
	β	**E**	**I**	K	K						
	β	**V**	**L**	F	L						
	β	**E**	**T**	Q	R						
	β	**I**	**L**	I	V						
	β	**V**	**L**	L	L						
		·	**N**	N	G						
	β	**D**	·	·	Y						
		·	S	S	N*						

[a] The equivalent residues in DtxR and spectrin are shown in bold; underlined residues are conserved in spectrin and Fyn; residues in direct contact with the ligand are marked * (Musacchio *et al.*, 1994). Assignment of secondary elements for DtxR by PROCHECK (Laskowski *et al.*, 1993).

SH3 domain of α-spectrin is shown in Figure 4. The SH3 fold has been found in a large variety of proteins without any significant sequence indentity. These include among others the BirA repressor (Wilson *et al.*, 1992), the PsaE polypeptide from photosystem I of cyanobacteria (Falzone *et al.*, 1994), the DNA binding protein Sso7D from an archaebacterium (Baumann *et al.*, 1994), and the DNA binding domain of HIV-I integrase (Lodi *et al.*, 1995).

Metal Binding Sites in the Co−DtxR. In the 2.8 Å Co^{2+}−DtxR structure (Qiu *et al.*, 1995), the first metal site was found to be coordinated tetrahedrally by His79, Glu83, His98, and a solvent molecule. It was not clear whether Glu83 provided one or both of its carboxylate oxygen atoms as metal ligands, and the nature of the solvent ligand was not identified at all. In the refined 2.0 Å resolution Co^{2+}−DtxR structure, these detailed features of the structure can now be defined (Figure 5a). The metal site site is tetrahedrally coordinated. The OE1 oxygen of Glu83 is found to be the metal ligand (Co^{2+}−Glu83 OE1, 1.9 Å); the OE2 is too far away at 3.3 Å to be considered as a ligand. Two nitrogen atoms are identified to be the ligand atoms from His79 and His98, with distances of 2.0 Å (Co^{2+}−His79 NE2) and 2.2 Å (Co^{2+}−His98 ND1), very acceptable as metal−ligand bond lengths. In the beginning of the refinement, the solvent ligand was modeled as a water molecule, which gave an unrealistic low temperature factor of 2 $Å^2$ in subsequent stages of refinement. The size and shape of the electron density suggested the presence of a bulkier and tetrahedral-like particle as a ligand to site 1 (Figure 5a). Considering the chemical environment of the molecule and the fact that the crystal was grown in the presence of 1.8 M ammonium sulfate, it was concluded that the solvent molecule was really a sulfate ion. Subsequent refinement as a sulfate with full occupancy resulted in very satisfactory temperature factors. The average *B*-factor of the five anion atoms is 35 $Å^2$, compared to the average of those of 17 $Å^2$ for the metal and the other ligands.

The Mn−DtxR Complex and the Sulfate at Metal Binding Site 1. The overall structure of the complex of DtxR with manganese is very similar to that of Co^{2+}−DtxR. The rms difference for the first two domains is 0.16 Å for the Cα's of 137 residues and 0.22 Å for all atoms. Clearly, the presence of one or two metal binding sites appears to have little effect on the structure of the first two domains of the repressor in the crystallization conditions used. The third domain of Mn^{2+}−DtxR is structurally close to that of Co^{2+}−

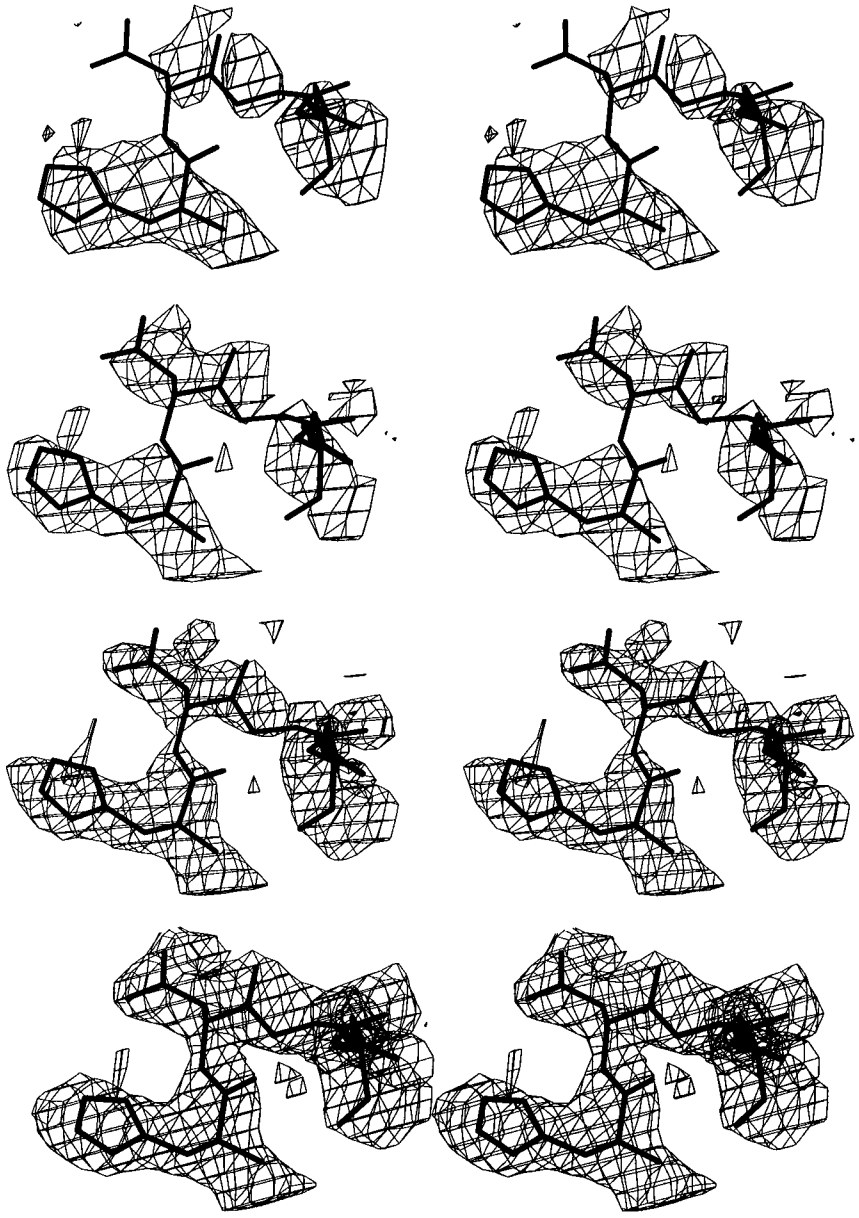

FIGURE 3: Stereoview of the $2F_o - F_c$ maps at 0.7σ level of the loop region showing residues 206−209. From top to bottom: (a) simulated annealing omit map calculated with data to 2.8 Å and a model excluding the third domain and the solvent molecules, (b) simulated annealing omit map using data to 2.8 Å and a model including the third domain and all water positions, (c) simulated annealing omit map using all data and our current model at 2.0 Å resolution, and (d) final $2F_o - F_c$ map. For the simulated annealing omit maps a region of 8 Å around residue 208 has been deleted in order to reduce model bias.

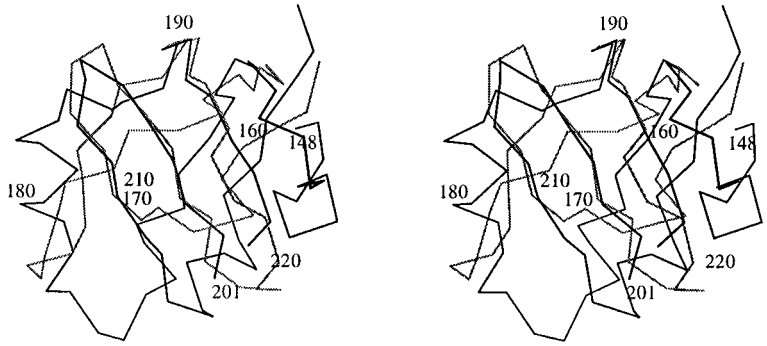

FIGURE 4: Least-squares superposition of 46 equivalent Cα atoms of the third domain of DtxR shown in black and the SH3 domain of spectrin depicted in gray; the rms deviation is 3.0 Å. The residue numbers refer to DtxR.

DtxR with an rms difference of 0.25 Å for 77 well-defined Cα atoms (0.35 Å for all atoms). Also, the average thermal parameters of the C-terminal domains are very similar: 56 Å^2 for Co^{2+}−DtxR and 65 Å^2 for Mn^{2+}−DtxR. Hence, in spite of flexibility of the loop by which the third domain is connected with the two other domains, its conformation is very similar in the two structures. Neither the difference in number and nature of the divalent cation nor the change from

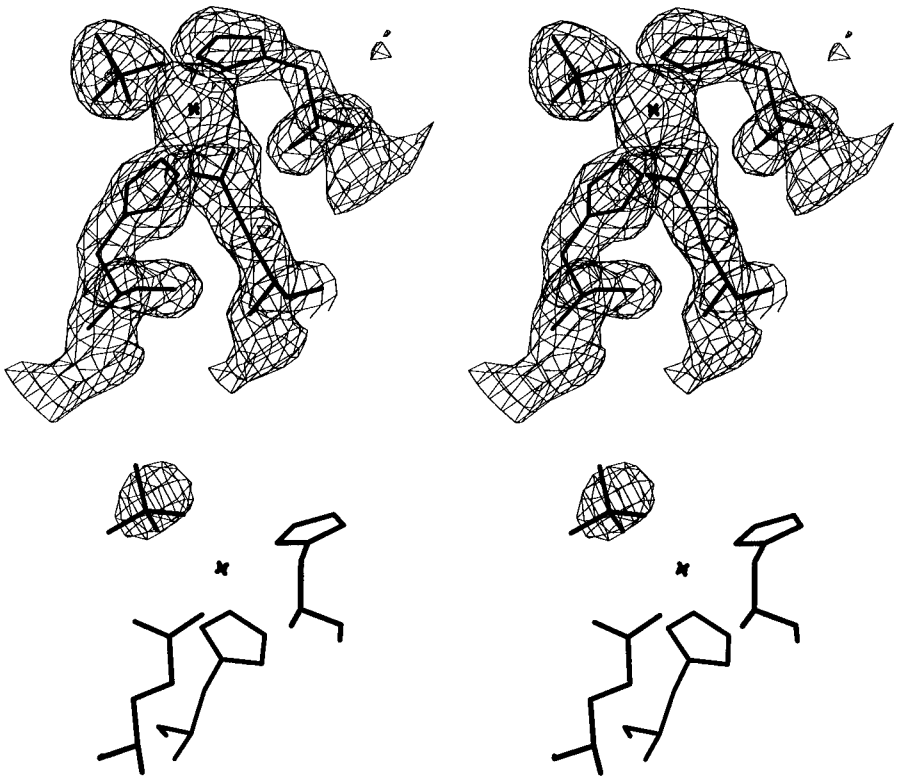

FIGURE 5: Stereoview of (a, top) the $2F_o - F_c$ map at 2σ level for metal binding site 1 showing the electron density for the sulfate anion and (b, bottom) $F_o(Mn, SeO_4) - F_o(Co, SO_4)$ difference map at 6σ level calculated with phases from the refined Co^{2+}−DtxR structure showing the electron density for the selenate. The maximum peak height at this position is 16σ.

Table 3: Geometry of the Metal Binding Sites in DtxR

	Co^{2+}−DtxR[a]	Mn^{2+}−SeO_4^{2-}−DtxR[a]
M1−NE2 His79	2.1	2.2
M1−ND1 His98	2.0	1.9
M1−OE1 Glu83	2.0	1.9
M1−O SO_4	2.1	1.9
M2−OE1 Glu105		2.5
M2−NE2 His106		2.5
M2−O Cys102		3.1
M2−O water		3.1

[a] Metal to ligand distances are given in angstroms.

sulfate to selenate has caused a significant difference between the two structures.

One of the major reasons for transferring the Mn^{2+}−SO_4^{2-}−DtxR crystals to 2.0 M selenate was to establish unequivocally that the fourth ligand of metal binding site 1 was provided by an oxygen of a sulfate ion. Because the Mn^{2+}−SO_4^{2-}−DtxR crystals are virtually isomorphous with those of Co^{2+}−SO_4^{2-}−DtxR, an F_o (Mn, SeO_4) − F_o (Co, SO_4) difference map was calculated with phases from the refined Co^{2+}−SO_4^{2-}−DtxR structure. There are two outstanding features in this difference map one peak of 16σ at the proposed sulfate ligand site and a second of 11σ at metal binding site 2. The F_o (Mn, SeO_4) − F_o (Co, SO_4) difference electron density map around metal position 1 is shown in Figure 5b. This result unambiguously confirms the presence of a sulfate ion which is partially substituted by the selenate in the sphere of coordination of metal site 1.

In the Mn^{2+}−SeO_4^{2-}−DtxR structure, the manganese at site 1 is coordinated in an identical manner as the cobalt in Co^{2+}−SO_4^{2-}−DtxR by the ND1 of His98, the OE1 of Glu83, the NE1 of His79, and O4 of the anion (Table 3, Figure 6a). The temperature factor of the Mn^{2+} ion is 17 Å^2 (compared to 18 Å^2 for Co^{2+}), and the average temperature factor of the SeO_4^{2-} ion is 25 Å^2 (compared to 35 Å^2 for SO_4 in Co^{2+}−SO_4^{2-}−DtxR). The rms deviation for the four atoms involved in liganding metal ions 1 in the two structures is 0.1 Å, whereas their average temperature factors are 21 Å^2 in the cobalt sulfate structure and 20 Å^2 in the manganese selenate complex. Hence, the difference in neither cation nor anion has a significant effect on the geometry of metal binding site 1.

The situation is different for metal binding site 2. In the Co^{2+}−SO_4^{2-}−DtxR crystals, no significant peak beyond that of a solvent molecule is present at this site. The solvent molecule is hydrogen bonded to OE1 of Glu105 (3.0 Å), NE2 of His106 (3.2 Å), carbonyl O of Cys102, and a water molecule (2.7 Å). In Mn^{2+}−SeO_4^{2-}−DtxR there is clearly an ion bond which, when refined with half-occupancy, gives a temperature factor of 23 Å^2, compared to 18 Å^2 for the fully occupied metal binding site 1 in Mn^{2+}−SeO_4^{2-}−DtxR. Metal binding site 2 in the 2.2 Å manganese structure is close to the second cadmium site previously reported for Cd^{2+}−SO_4^{2-}−DtxR (Qiu *et al.*, 1995): after superposition of the Cα atoms of the two structures, the Mn^{2+} differs 0.7 Å from the Cd^{2+} position. Also, the ligands are identical in the Cd and Mn structures with protein ligands: the carbonyl oxygen of Cys102, the OE1 of Glu105, and the NE2 of His106 (Figure 6b). In addition, there is a well-defined solvent molecule as a fourth ligand. This solvent molecule obtains a temperature factor of 36 Å^2 when refined as a water molecule with full occupancy. Due to the higher resolution of Mn^{2+}−SeO_4^{2-}−DtxR compared to the cadmium structure of Qiu *et al.* (1995) we have now a more accurate picture of this metal binding site (Figure 6b, Table 3).

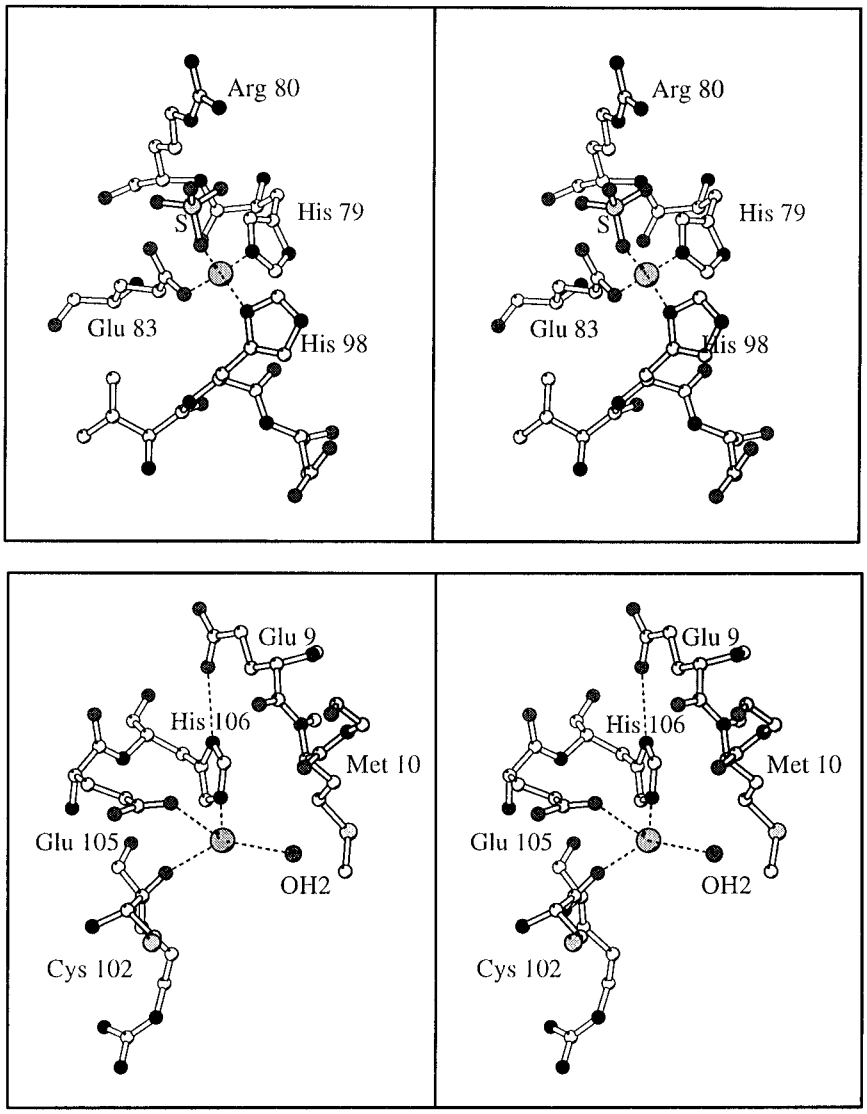

FIGURE 6: Stereoviews of the metal binding sites: (a, top) refined Co^{2+} and sulfate structure; (b, bottom) refined metal binding site 2 in the Mn^{2+} structure.

DISCUSSION

Overall Structure. From the close similarity of the $Co^{2+}-SO_4^{2-}-$DtxR and $Mn^{2+}-SeO_4^{2-}-$DtxR structures, and of the two N-terminal domains in $Co^{2+}-SO_4^{2-}-$DtxR, $Mn^{2+}-SeO_4^{2-}-$DtxR (this work), $Cd^{2+}-SO_4^{2-}-$DtxR and "1 mM EDTA$-SO_4^{2-}-$DtxR" (Qiu *et al.*, 1995), it is clear that the nature of the divalent cation (and the change from selenate to sulfate) has very little effect on the overall structure of the diphtheria toxin repressor. This even includes differences in occupancy in the two metal binding sites which ranges from low for both metal sites in the "1 mM EDTA" structure to one full and one half-occupied in the case of $Mn^{2+}-SeO_4^{2-}$-DtxR. In addition, the third domains are very similar even though the flexible linker between domains 2 and 3, coupled with the absence of contacts of domain 3 with either of these domains, suggests that the positions of domain 3 with respect to domains 1 and 2 can vary significantly in different crystal forms. Some evidence for this possibility is obtained from preliminary results in different crystal forms (X. Qiu, E. Pohl, and W. G. J. Hol, unpublished).

The Third Domain, a Bacterial SH3 Fold. From our model, it is quite clear that the third domains of the DtxR dimer are very distant from the putative DNA binding region and metal binding sites (Figure 2), which raises the possibility that the domains are dispensable for the repressor activity. In fact, six mutations in the domain have been reported that do not affect the repressor activity (Boyd *et al.*, 1992). However, it is known that structural elements of proteins other than the major DNA recognition sites can bind to DNA after conformational changes and contribute to the overall stability or specificity of the protein−DNA complexes. Examples are the N-terminal arm of the λ repressor (Jordan & Pabo, 1988) and the C-terminal helix of the *Bam*HI endonuclease (Newman *et al.*, 1995). There are positively charged regions on the surface of the third domain which might interact with the phosphate ribose backbone of DNA in the DtxR−DNA complex. However, the electrostatic surface potential calculated using the program GRASP (Nicholls *et al.*, 1991) does not show any obvious extensive electropositive patches for DNA binding. The high mobility in the crystal form of metal-containing DtxR indicates that the third domain might be able to undergo a conformational change. Therefore, we should not exclude the possibility that the domain may be able to wrap around to interact with the DNA after a major conformational change utilizing the considerable flexibility of the linker region. The sequence

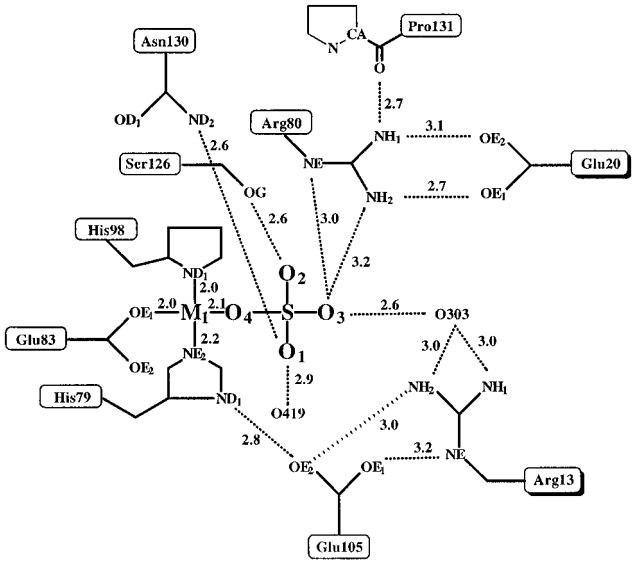

FIGURE 7: Schematic drawing of the hydrogen-bonding network involving the sulfate ion. All the distances are shown in units of Ångstroms. The first site metal is labeled as M1. Solid lines are covalent bonds, while dotted lines are salt bridges or hydrogen bonds. Residues from the first domain are labeled in shadowed boxes. O301 represents a solvent molecule that gives a refined temperature factor of 23 Å^2. Note the careful liganding of the sulfate by protein side chains.

alignment to the SH3 of α-spectrin and to the two tyrosine kinase SH3 domains, Fyn and ABL, is given in Table 2. For Fyn and ABL the crystal structure in complex with a proline-rich peptide has been determined at high resolution by Musacchio *et al.* (1994). The solution structure of the SH3 domain of Src in complex with proline-rich peptides has been determined by Yu *et al.* (1992) and Feng *et al.* (1994). None of the residues involved in direct contact to the peptide in Fyn or ABL are conserved. Thus it is very unlikely that the third domain of DtxR binds peptides in a way similar to that of other SH3 domains. Yet, the possibility exists that the role of the third domain might involve interaction with other proteins. The function of the third domain remains most intriguing.

Metal Binding Site 1 and the Possible Role of Phosphate as Ligand. This metal binding site is well occupied in the Co, Cd, Mn, Ni, Zn, and Fe DtxR structures determined by Qiu *et al.* (1995) and in this work. The surprising fact is that the fourth ligand is a sulfate ion oxygen in the $P3_121$ crystal form we have studied so far. The sulfate ion is very well ligated by protein atoms and provides several contacts to other domains of the protein (Figure 7). Biochemical evidence has been presented for a binding of one Ni^{2+} per monomer (Wang *et al.*, 1994). The binding constant has been determined from the quenching of intrinsic tryptophan fluorescence with a half-saturation of 9×10^{-7}M (Tao *et al.*, 1995). Since a second metal binding site was observed to be only partially occupied in the 5 mM $Cd^{2+}-SO_4^{2-}-$DtxR and 5 mM $Mn^{2+}-SeO_4^{2-}-$DtxR structures, it seems clear that metal binding site 1 is a high-affinity site and metal site 2 a low-affinity site. However, the presence of 2 M sulfate (or selenate) is quite far from physiological conditions, and this has to be taken carefully into account.

There appear to be two distinct possibilities. One is that sulfate and selenate mimic a phosphate ion which, present at 50 mM in mammalian cells (Brock *et al.*, 1984), is the physiological ligand of metal 1. The difference between the sulfate and monohydrogen phosphate ion is a very small difference in geometry plus an extra hydrogen in HPO_4^{2-}. The geometric difference between the two anions is unlikely to play a significant role since the ion is in contact with quite flexible side chains (OD1 of Asn130, OG of Ser126) and a solvent ion (Figure 7) which can easily rearrange to accommodate the small structural difference between the two anions. Also, the extra hydrogen of HPO_4^{2-} appears to be no serious problem since one oxygen of sulfate is in contact with solvent, and one with a hydroxyl group of Ser126, and hence the OH group of the phosphate ion could be accommodated. If this were the case, then phosphate might be an intrinsic ligand of metal 1 and assist in coordinating Fe^{2+} at this site under physiological conditions. It would act as a "co-corepressor". The affinity of DtxR for metals then becomes dependent on the concentration of HPO_4^{2-} in the solution, and clearly detailed further investigations are required to definitely prove the role of phosphate in the functioning of DtxR.

The second possibility is that the presence of 2 M sulfate has created a binding site which is purely an artifact of the crystallization conditions used. Evidence in support for this comes from the fact that we have yet not been able to obtain crystals suitable for X-ray diffraction in the absence of sulfate (and neither in the presence of phosphate). This is not very strong evidence, however, since crystal growth can be exquisitely sensitive on the presence, type, and concentration of salt. It is obvious that the high-resolution DtxR crystal structure provides a platform for mutagenesis experiments to investigate this issue by verifying not only the ligands of metal binding site 1 but also the sulfate-coordinating side chains. Recently Ding *et al.* (1996) showed that point mutations of the ligands of metal binding site 1 had little or no effect on the activity of the repressor whereas mutations of ligands of metal binding site 2 abolish the metal repressor activity. These results suggest that metal binding site 2 is of major importance for repressor activation as was considered by Qiu *et al.* (1995).

Metal Binding Site 2. The occupancy of site 2 appears to be erratic: it is well occupied (~50%) in the 5 mM $Mn^{2+}-SeO_4^{2-}-$DtxR structure described in this paper, weakly but definitely occupied in the 5 mM $Cd^{2+}-SO_4^{2-}-$DtxR structure (Qiu *et al.*, 1995), and virtually not occupied in the $Ni^{2+}-SO_4-$DtxR, $Fe^{2+}-SO_4^{2-}-$DtxR and "1 mM EDTA$-SO_4^{2-}-$DtxR" structures. The position is also occupied in the mercury derivatives found by Qiu *et al.* (1995). Why are these occupancies different and what is the physiological relevance of this site, if any?

A quite surprising observation in the Cd and Mn structures is that the SG of Cys102 is not a ligand of the metal bound at site 2. Instead, and quite intriguingly, the main chain carbonyl oxygen of Cys102 is a ligand of metal 2. Saturation mutagenesis studies of Tao and Murphy (1993) showed that Cys102 could only be replaced by an Asp residue and yield a DtxR structure which retains (some of) its metal-activated DNA binding. This suggests that this residue either (i) is providing a direct ligand (quite likely its SG but, as observed in our crystal structures, also possibly its carbonyl oxygen) or (ii) is in contact with a ligand [we have earlier pointed out that the SG of Cys102 is in contact with His 98, a direct ligand of site 1 (Qiu *et al.*, 1995)] or (iii) is no ligand but is affecting a functional conformational change which DtxR has to undergo in order to exhibit activity. Recently, the

crystal structure of the Cys102Asp variant complexed with Ni^{2+} has been determined by Ding *et al.* (1996). In this mutant structure metal binding site 1 is occupied with the same ligands as in our structures although the metal−ligand distances differ significantly. The second metal binding site is ligated by a nitrogen of His106, a carboxylate oxygen of Glu105, the main chain carbonyl of Asp120, a carboxylate oxygen of the mutated Asp102, and the sulfur from Met10 with a distance of 2.7 Å. In the Cys102Asp mutant and in our wild-type structures metal binding site 2 differs in certain aspects, as expected since the mutation involves a metal ligand. However, many features are quite similar.

One possible explanation for the variations observed at metal site 2 in the various crystal structures we have solved of wild-type DtxR in the presence of functional divalent cations might be a chemical modification of its sulfhydryl group. In the 2.8 Å structures reported by Qiu *et al.* (1995) some evidence for oxidation was observed for the SG of Cys102. At higher resolution, the difference electron densities in both Co^{2+}−SO_4^{2-}−DtxR and Mn^{2+}−SeO_4^{2-}−DtxR structures show a strong peak approximately 2.0 Å from the SG of Cys102. Although it is difficult to identify an unknown chemical group crystallographically, the sulfur to peak distance of 2.0 Å and a CB−SG−peak angle of approximately 95° suggest that the SG might be covalently linked to a second sulfur. Refinement of the extra SD leads to a temperature factor of 28 $Å^2$, compared to 23 $Å^2$ for the adjacent SG. This suggests the possibility that a mixed disulfide has been formed. The formation of mixed disulfides from free cysteines has been found previously in the crystal structure of ferredoxin II (Kissinger *et al.*, 1991). It should be noted that no significant density whatsoever is present beyond the SD of Cys102, and hence, we have no crystallographic information regarding the moiety which might be attached to the SG and is possibly freely rotating in the solvent.

It is clear that the importance of metal binding site 2 needs detailed further investigations. Obviously, the occurrence of the chemical modification of the SG of Cys102 (either by oxidation, mixed disulfide formation, or other process) might prevent this potential metal ligand from interacting with a metal ion as would have occurred under physiological conditions. Hence, under the reducing conditions in the *C. diphtheriae* cell, it is possible that an alternative metal binding site exists which is somewhat different from metal binding site 2 as seen in our Cd^{2+}− and Mn^{2+}−DtxR crystal structures. Alternatively, the diphtheria toxin repressor might contain a cysteine residue which is poised for chemical modifications, and the crystal structures reveal the beginning of the mechanisms of controlling the metal affinity of DtxR which might be as surprising as complex.

CONCLUSION

The high-resolution structures of Co^{2+}−DtxR in sulfate and Mn^{2+}−DtxR in selenate have established a well-defined structure for all three domains of the repressor. The presence of a well coordinated sulfate ion as a ligand of metal binding site 1 has been revealed, and DtxR shows virtually the same second metal binding site as previously seen in Cd^{2+}−DtxR (Qiu *et al.*, 1995). The sulfate anion near metal binding site 1 is involved in a large hydrogen-bonding network that introduces several crucial connections to the first domain residues. The exact role of this sulfate with the intriguing possibility that it mimics a physiologically relevant phosphate co-corepressor, needs to be established. Also, metal binding site 2 is still surrounded by mysteries. The reasons for its variable occupancy and the nature and effect of possible chemical modifications of the nearby, but not liganding, sulfhydryl group of Cys102 will need to be unraveled before the exact mechanism by which this Fe-dependent repressor functions can be elucidated. Mutagenesis studies showed that Cys102 is essential for activation (Tao & Murphy, 1993) even though the side chain of this residue is not directly involved in metal coordination of the two metal binding sites. One possible explanation is that residue 102 has been chemically modified during preparation or crystallization, thus preventing metal coordination. Mutational studies also suggest that metal binding site 2 is the major factor in metal-activated DNA binding (Ding *et al.*, 1996) as was also considered by Qiu *et al.* (1995).

The positions of the two DNA binding helices, and therefore the distance of the helices, are controlled by the the relative orientation of the monomers with respect to each other. The metal positions can act as pivotal points for rearrangement of the domains or the monomers. From the crystal structures determined so far it is not clear which metal position is responsible for activation of the repressor; it is also possible that both positions are important. Further structural studies on protein−DNA complexes are neccessary to investigate the role of metal binding as well as the role of the C-terminal third domain.

REFERENCES

Barksdale, L. (1970) *Corynebacterium diphtheriae* and its relatives, *Bacteriol. Rev. 34*, 387−422.

Baumann, H., Knapp, S., Lundbäck, T., Ladenstein, R., & Härd, T. (1994) Solution structure and DNA-binding properties of a thermostable protein from the archaeon *Sulfolobus solfataricus*, *Nat. Struct. Biol. 1*, 808−819.

Boyd, J. M., Oza, M. N., & Murphy, J. R. (1990) Molecular cloning and DNA sequence analysis of a diphtheria *tox* iron-dependent regulatory element (*dtxR*) from *Corynebacterium diphtheriae*, *Proc. Natl. Acad. Sci. U.S.A. 87*, 5968−5972.

Boyd, J. M., Hall, K. C., & Murphy, J. R. (1992) DNA sequences and characterization of dtxR alleles from *Corynebacterium diphtheriae* PW8(−), 1030(−) and C7hm 723(−), *J. Bacteriol. 174*, 1268−1272.

Brennan, R. G. (1993) The winged-helix DNA-binding motif: another helix-turn-helix takeoff, *Cell 74*, 773−776.

Brock, T. D., Smith, D. W., & Madigan, T. M. (1984) *Biology of Microorganism*, Prentice-Hall, Inc., Englewood Cliffs, NJ.

Brünger, A. T., Kuriyan, J., & Karplus, M. (1987) Crystallographic R factor refinement by molecular dynamics, *Science 235*, 458−460.

Collaborative Computational Project, Number 4 (1994) The CCP4 Suite: programs for protein crystallography, *Acta Crystallogr. D50*, 760−763.

Ding, X., Zeng, H., Schiering, N., Ringe, D., & Murphy, J. R. (1996) Identification of the primary metal ion-activation sites of the diphtheria tox repressor by X-ray crystallography and site-directed mutational analysis, *Nat. Struct. Biol. 3*, 382−387.

Falzone, C. J., Kao, Y. H., Zhao, J., Bryant, D. A., & Lecomte, J. T. J. (1994) Three-dimensional Solution Structure of PsaE from the *Cyanobacterium synechococcus* sp. Strain PCC 7002, a Photosystem I Protein That Shows Structural Homology with SH3 domains, *Biochemistry 33*, 6052−6062.

Feng, S., Chen, J. K., Yu, H., Simon, J. A., & Schreiber, S. L. (1994) Two Binding Orientations for Peptides to the Src SH3 Domain: Development of a General Model for SH3-Ligand Interactions *Science 266*, 1241−1247.

Hodel, A., Kim, S.-H., & Brünger, A. T. (1992) Model Bias in Macromolecular Structures, *Acta Crystallogr. A48*, 851−858.
Holm, L., & Sander, C. (1993) Protein Structure Comparison by Alignment of Distance Matrices, *J. Mol. Biol. 233*, 123−138.
Jones, T. A., Zou, J. Y., Cowan, S. W., & Kjeldgaard, M. (1991) Improved methods for building protein models in electron density maps and the location of errors in these models, *Acta Crystallogr. A47*, 110−119.
Jordan, S. R., & Pabo, C. O. (1988) Structure of the lambda complex at 2.5 Å resolution: details of the repressor-operator interactions, *Science 242*, 893−899.
Kissinger, C. R., Sieker, L. C., Adman, E. T., & Jensen, L. H. (1991) Refined Crystal Structure of Ferredoxin II from *Desulfovibrio gigas* at 1.7 Å, *J. Mol. Biol. 219*, 693−715.
Kraulis, P. (1991) MOLSCRIPT: a program to produce both detailed and schematic plots of protein structures, *J. Appl. Crystallogr. 24*, 946−950.
Lamzin, V. S., & Wilson, K. S. (1993) Automated refinement of protein models, *Acta Crystallogr. D49*, 129−147.
Laskowski, R. A., MacArthur, M. W., Morris, A. L., & Thornton, J. M. (1993) PROCHECK: a program to check the stereochemical quality of protein structures, *J. Appl. Crystallogr. 26*, 283−291.
Litwin, C. M., & Calderwood, S. B. (1993) Role of iron in regulation of virulence genes, *Clin. Microbiol. Rev. 6*, 137−149.
Lodi, P. J., Ernst, J. A., Kuszewski, J., Hickmann, A. B., Engelmann, A., Craigie, R., Clore, G. M., & Gronenborn, A. M. (1995) Solution Structure of the DNA Binding Domain of HIV Integrase, *Biochemistry 34*, 9826−9833.
Musacchio, A., Noble, M. E. M., Pauptit, R., Wierenga, R. K., & Saraste, M. (1992) Crystal structure of a Src-homology-3 (SH3) domain, *Nature 359*, 851−855.
Musacchio, A., Saraste, M., & Wilmanns, M. (1994) High resolution crystal structures of tyrosin kinase SH3 domains complexed with proline rich peptides, *Nat. Struct. Biol. 1*, 546−551.
Newman, M., Strzelecka, T., Dorner, L., Schildkraut, I., & Aggarwal, A. K. (1995) Structure of Bam HI endonuclease bound to DNA: partial folding and unfolding on DNA binding, *Science 269*, 656−663.
Nicholls, A., Sharp, K., & Honig, B. (1991) Protein folding and association; insights from the interfacial and thermodynamic properties of hydrocarbons, *Proteins 11*, 281−296.
Oguiza, J. A., Tao, X., Marcos, A. T., Martin, J. A., & Murphy, J. R. (1995) Molecular cloning, DNA sequence analysis and characterization of the *Corynebacterium diphtheriae* dtxR homolog from *Brevibacterium lactofermentum*, *J. Bacteriol. 177*, 465−467.
Qiu, X., Verlinde, C. L. M. J., Zhang, Z., Schmitt, P., Homes, R. K., & Hol, W. G. J. (1995) Three-dimensional structure of the diphtheria toxin repressor in complex with divalent cation co-repressors, *Structure 3*, 87−100.
Read, R. J. (1986) Improved Fourier Coefficients for Maps using Phases from Partial Structures with errors, *Acta Crystallogr. A42*, 140−149.
Schiering, N., Tao, X., Zeng, H., Murphy, J. R., Petsko, G. A., & Ringe, D. (1995) Structures of the apo- and the metal ion-activated forms of the diphtheria toxin repressor from *Corynebacterium diphtheriae*, *Proc. Natl. Acad. Sci. U.S.A. 92*, 9843−9850.
Schmitt, M. P., & Holmes, R. K. (1993) Analysis of diphtheria toxin repressor-operator interactions and characterization of a mutant repressor with decreased binding activity for divalent metal, *Mol. Microbiol. 9*, 173−181.
Schmitt, M. P., & Holmes, R. K. (1994) Cloning, sequence and footprint analysis of two promotor operators from *Corynebacterium diphtheriae* that are regulated by the diphtheria toxin repressor (DtxR) and Iron, *J. Bacteriol*., 1141−1149.
Schmitt, M. P., Twiddy, E. M., & Holmes, R. K. (1992) Purification and characterization of the diphtheria toxin repressor, *Proc. Natl. Acad. Sci. U.S.A. 89*, 7576−7580.
Schmitt, M. P., Redich, M., Doukhan, C., Smith, I., & Holmes, R. K. (1995) Characterization of an iron dependent regulatory protein (IdeR) of *Mycobacterium tuberculosis* as a functional homolog of DtxR from *Corynebacterium diphtheriae*, *Infect. Immun. 63*, 4284−4289.
Shultz, S. C., Shields, G. C., & Steitz, T. A. (1991) Crystal structure of a CAP-DNA complex: the DNA is bent by 90 degrees, *Science 253*, 1001−1007.
Tao, X., & Murphy, J. R. (1992) Binding of the metalloregulatory protein DtxR to the diphtheria tox operator requires a divalent heavy metal ion and protects the palindromic sequence from Dnase I digestion, *J. Biol. Chem. 267*, 21761−21764.
Tao, X., Schiering, N., Zeng, H., Ringe, D., & Murphy, J. R. (1994) Iron, DtxR, and the regulation of diphtheria toxin expression, *Mol. Microbiol. 14*, 191−197.
Wang, Z., Schmitt, M. P., & Holmes, R. K. (1994) Characterization of mutations that inactivate the diphtheria toxin repressor gene (*dtxR*), *Infect. Immun. 62*, 1600−1608.
Weinberg, E. D. (1993) The development of awareness of iron-withholding defense, *Prospect. Biol. Med. 36*, 215−221.
Wilson, K. P., Shewchuk, L. M., Brennan, R. G., Otsuka, A. J., & Matthews, B. W. (1992) *Escherichia coli* biotin holoenzyme synthetase/*bio* repressor crystal structure delineates the biotin and DNA-binding domains, *Proc. Natl. Acad. Sci. U.S.A. 89*, 9257−9261.
Yu, H., Rosen, M. K., Shin, T. B., Seidel-Dugan, C., Brugge, J. S., & Schreiber, S. L. (1992) Solution Structure of the SH3 Domain of Src and Identification of its Ligand-Binding Site, *Science 258*, 1665−1668.

BI960861D